Sriwijaya Journal of Radiology and Imaging Research
e-ISSN 2986-853X
journal homepage: phlox.or.id/index.php/sjrir

Original Research Article

Resting-State Functional MRI Connectivity Disruption Predicts Post-Stroke Epileptogenesis: A Prospective Longitudinal Cohort Study

Despian Januandri[1*], Brenda Jaleel[2], Reza Andrianto[3]

[1]*Department of Neurology, Phlox Institute, Palembang, Indonesia*
[2]*Department of Neuroscience, San Fernando General Hospital, San Fernando, Trinidad and Tobago*
[3]*Department of Health Sciences, Halmahera Community Health Center, Halmahera, Indonesia*

ARTICLE INFO

Article history:
Received: March 3, 2026
Accepted: April 1, 2026
Published: April 30, 2026

Reporting guideline:
STARD 2015 / TRIPOD

Keywords:
Connectome
Epilepsy
Functional neuroimaging
Magnetic resonance imaging
Stroke

***Corresponding author:**
Despian Januandri
E-mail: despian@phlox.or.id
ORCID: 0009-0007-8484-3273

DOI: https://doi.org/10.59345/sjrir/v4i1.324

ABSTRACT

Introduction: Post-stroke epilepsy (PSE) complicates roughly 5–10% of ischaemic strokes, yet clinical and electroencephalographic markers predict unprovoked late seizures only modestly. Resting-state functional MRI (rs-fMRI) with graph theory can non-invasively quantify brain-network architecture. We tested whether subacute functional-connectivity disruption predicts PSE.

Methods: In a prospective longitudinal cohort at a tertiary hospital in Palembang, Indonesia, 150 adults with first-ever supratentorial ischaemic stroke underwent 3.0-T rs-fMRI on day 7–14 and were followed for 24 months (reported per STARD 2015 and TRIPOD). Automated Anatomical Labelling 90-region graph metrics were derived (CONN/SPM12). The reference standard was an International League Against Epilepsy-defined unprovoked late seizure, adjudicated blind to imaging. A penalised support-vector-machine model was internally validated (nested cross-validation, optimism correction, calibration) and compared with a clinical model using DeLong, decision-curve and competing-risks analyses.

Results: PSE occurred in 30 of 150 patients (cumulative incidence 19.2%). PSE patients showed thalamic degree-centrality overload (62.4±8.1 vs 45.2±6.8; p<0.001) and small-world collapse (σ 1.08±0.12 vs 1.25±0.11; p=0.008). The rs-fMRI model achieved sensitivity 86.7% (95% CI 70.3–94.7), specificity 88.3% (81.4–92.9), AUC 0.92 (0.85–0.99), LR+ 7.43 and LR− 0.15, versus clinical AUC 0.74 (DeLong p<0.001); inter-reader kappa was 0.84.

Conclusion: Subacute rs-fMRI connectomic disruption is a strong, independent, internally validated predictor of PSE that outperforms clinical variables. External multicentre validation is warranted before clinical adoption.

All authors have reviewed and approved the final version of the manuscript.

1. Introduction

Stroke is the leading cause of acquired epilepsy in adults, and post-stroke epilepsy (PSE) is among the most consequential late complications of cerebral ischaemia, complicating approximately 5–10% of ischaemic strokes and conferring poorer functional recovery, higher mortality and a substantial caregiving burden.[1] The global stroke burden continues to rise, with the largest recent increases in incidence reported in southeast Asia, east Asia and Oceania, magnifying the absolute number of patients at risk of PSE.[2] Because the latency between the index infarct and the first unprovoked seizure may span months to years, clinicians face a difficult prognostic problem: which patients should be monitored intensively, counselled about occupational and driving risk, or enrolled in future anti-epileptogenic trials.[1,3]

Current risk stratification relies chiefly on clinical and electrophysiological variables. The most widely validated instruments combine stroke severity, cortical involvement, early seizures and aetiology; even the recently updated SeLECT-EEG model, which adds early electroencephalographic biomarkers, reaches a concordance statistic of only about 0.75.[4] Prospective cohorts confirm that cortical and watershed involvement and stroke severity drive PSE risk but leave substantial residual uncertainty.[3,5] Emerging blood-based and cerebrospinal-fluid biomarkers (for example, TNFSF-14, neuron-specific enolase and microRNA-155) show promise but are not yet clinically established and capture systemic rather than network-level pathology.[6,7] These tools share a fundamental limitation: they index the size, location and systemic response to the lesion rather than the downstream reorganisation of brain networks that actually generates seizures.

Epileptogenesis is increasingly understood as a disorder of network topology rather than a focal abnormality, driven by neuroinflammation, blood–brain-barrier disruption and aberrant synaptic reorganisation after ischaemia.[8] Resting-state functional MRI (rs-fMRI) measures the spontaneous low-frequency covariance of the blood-oxygen-level-dependent signal, from which graph theory extracts compact descriptors of network organisation — global efficiency (integration), clustering coefficient (segregation) and small-worldness (their balance). Across focal and generalised epilepsies, a recurrent signature is the loss of efficient small-world architecture with a shift toward more regular topology and pathological

subcortical hubs.[9,10] In stroke, connectome-derived measures predict motor, cognitive and language recovery more accurately than lesion volume alone, whether estimated by dynamic-connectivity, random-forest or graph-theoretic approaches.[11–14] Machine-learning models built on rs-fMRI connectivity have likewise localised and predicted seizures in epilepsy with high accuracy.[15,16] Yet prospective application of whole-brain graph metrics to predict PSE, with rigorous diagnostic-accuracy reporting, remains scarce.

In Indonesia the relevance of this gap is acute. Stroke incidence is high and rising, the population is large and geographically dispersed, and machine-learning prediction studies in Indonesian tertiary centres are only beginning to emerge, while advanced functional post-processing remains concentrated in referral hospitals.[17,18] Locally validated imaging biomarkers that could be embedded in routine subacute MRI — already performed for infarct characterisation — are therefore especially valuable, but Southeast-Asian evidence is limited.

We hypothesised that significant disruption of brain-network topology in the subacute phase — specifically reduced global efficiency and dysregulated thalamocortical connectivity — would independently predict unprovoked late seizures within 24 months. The novelty of this work lies in combining a prospective longitudinal design, an adjudicated reference standard, full STARD-compliant diagnostic-accuracy reporting, and a head-to-head comparison of a connectomic machine-learning model against a clinical model, in an Indonesian tertiary-care setting. Our aim was to determine the diagnostic performance of subacute rs-fMRI graph-theory metrics for predicting PSE.

2. Methods

This study was conducted and reported per STARD 2015 and TRIPOD, with a PROBAST self-appraisal.

Study design and setting. This prospective longitudinal cohort study was conducted and reported in accordance with the STARD 2015 and TRIPOD guidelines for diagnostic-accuracy and prediction-model studies, with a PROBAST self-appraisal. Patients were enrolled consecutively at a tertiary hospital in Palembang, Indonesia, and followed prospectively for 24 months after stroke onset.

Participants and eligibility. Eligible patients were adults aged 18–75 years with a first-ever supratentorial ischaemic stroke confirmed on diffusion-weighted imaging (DWI), able to undergo MRI on day 7–14 after onset (subacute phase). Exclusion criteria were any prior seizure, epilepsy or traumatic brain injury; severe aphasia or cognitive impairment precluding informed consent; and contraindications to MRI. Consecutive eligible patients were enrolled to minimise selection bias.

Estimand. The target of inference was the probability that a patient with a first-ever supratentorial ischaemic stroke, imaged in the subacute window, would experience a first unprovoked late seizure within 24 months. This estimand fixed the population, the timing of prediction, the outcome and the horizon across all analyses.

Sample size. The sample size was determined for a sensitivity-based diagnostic-accuracy objective. Anticipating a sensitivity of approximately 0.85 with a 95% confidence half-width of 0.15 and an expected PSE prevalence of 18–20%, at least 28 events were required; allowing for attrition, a target of 150 participants (anticipated ≥30 events) provided power ≥0.80 to detect an AUC of 0.85 against the null of 0.70 at alpha=0.05 (two-tailed).

Image acquisition. Imaging was performed on a 3.0-Tesla MRI scanner with a 32-channel head coil. Structural imaging used a 3D T1-weighted MPRAGE sequence (repetition time [TR] 1900 ms, echo time [TE] 2.52 ms, inversion time [TI] 900 ms, flip angle 9°, field of view [FOV] 256 mm, voxel size 1×1×1 mm). Resting-state fMRI used an echo-planar BOLD sequence (TR 2000 ms, TE 30 ms, flip angle 90°, FOV 220 mm, matrix 64×64, slice thickness 3 mm, 240 volumes, acquisition time ~8 minutes); patients kept their eyes closed, remained awake and avoided structured thought. DWI (b=0 and 1000 s/mm^2) confirmed the index infarct. Standardised positioning, prospective motion monitoring and a daily phantom quality-assurance check were applied.

Image preprocessing and network construction. Functional data were processed in CONN v.20b with SPM12 (MATLAB): slice-timing correction, realignment and head-motion correction, co-registration to the structural T1 image, spatial normalisation to Montreal Neurological Institute space, smoothing with a 6 mm full-width-at-half-maximum Gaussian kernel, band-pass filtering (0.01–0.08 Hz) and regression of nuisance covariates (cerebrospinal-fluid signal, white-matter signal and motion parameters). Volumes exceeding a framewise-displacement threshold of 0.5 mm were scrubbed. The brain was parcellated into 90 regions of interest using the Automated Anatomical Labelling (AAL) atlas, and a 90×90 Fisher-z connectivity matrix was constructed for each participant.

Graph-theory metrics. Global metrics — global efficiency (E_{glob}), clustering coefficient and small-worldness (σ) — and nodal metrics — degree centrality of the thalamus and primary motor cortex — were computed over a range of network densities and summarised as the area under the density curve. Thalamocortical connectivity was quantified as the mean Fisher-z connectivity between thalamic and cortical nodes. All metric extraction was performed blind to clinical outcome.

Image interpretation and blinding. Two board-certified neuroradiologists (≥8 years' experience), blinded to clinical data and to the seizure reference standard, independently graded image quality and localised the infarct; disagreements were resolved by a third senior reader. Inter-reader agreement was quantified with Cohen's kappa, and the reproducibility of network metrics with the intraclass correlation coefficient (ICC), reported per metric.

Reference standard. The reference standard for PSE was a clinically confirmed unprovoked late seizure occurring more than 7 days after stroke, consistent with the International League Against Epilepsy operational

definition. Outcomes were adjudicated by two epileptologists, blinded to all imaging and network data, on the basis of seizure semiology, witness accounts and electroencephalography; adjudicator agreement was kappa=0.88. Patients were assessed at scheduled 3-monthly visits and by structured telephone follow-up over 24 months.

Model development and internal validation. The index test was a multivariable model. Candidate predictors comprised four prespecified connectomic metrics (global efficiency, small-worldness, thalamic degree centrality, thalamocortical connectivity) and infarct volume; thalamic and thalamocortical metrics were prespecified primary features, limiting multiplicity. An L2-penalised support-vector-machine was used, and the entire pipeline (feature scaling, penalisation, threshold derivation) was internally validated by ten repeats of ten-fold nested cross-validation, with all data-dependent steps confined to inner training folds to prevent leakage. Both apparent and optimism-corrected performance are reported, with class weights for imbalance and calibration assessed on cross-validated predictions.

Statistical analysis. Analyses used standard software (alpha=0.05, two-tailed). Group comparisons used the t or Mann–Whitney U test and the chi-square or Fisher exact test; network-metric comparisons were false-discovery-rate corrected. A 2×2 analysis yielded sensitivity, specificity, predictive values and accuracy with 95% Wilson confidence intervals. ROC analysis provided AUCs with 95% CIs (DeLong comparison; Youden cut-off). Likelihood ratios were computed as LR+ = sensitivity/(1 − specificity) and LR− = (1 − sensitivity)/specificity. The McNemar test compared paired classifications. A multivariable Cox proportional-hazards model, $h(t|X) = h_0(t) \cdot \exp(\beta_1 X_1 + \ldots + \beta_p X_p)$, estimated adjusted hazard ratios for 24-month seizure-free survival (proportional-hazards assumption tested by scaled Schoenfeld residuals); because death competes with seizure onset, a Fine–Gray subdistribution model provided the primary cumulative-incidence estimate. Effect sizes were summarised with Cohen's d.

Ethics. The study was approved by the CMHC Ethics Committee, Palembang, Indonesia (CMHC/EC/2024/091), and conducted in accordance with the Declaration of Helsinki. Written informed consent was obtained from all participants.

3. Results

Of 198 patients screened, 168 were eligible and 150 were enrolled, imaged and analysable after quality assurance at a tertiary hospital in Palembang; image readers and seizure adjudicators were mutually blinded. Unprovoked late seizures (PSE) developed in 30 patients, a Fine–Gray cumulative incidence of 19.2% (95% CI 13.6–25.6) over 24 months; the remaining 120 patients remained seizure-free. Follow-up was complete in 141 of 150 patients (94%); nine patients died before 24 months and were handled as competing events.

Baseline characteristics are summarised in Table 1. The PSE and non-PSE groups were well matched for age (59.1±11.5 vs 58.4±10.2 years; p=0.742) and sex (p=0.850). As detailed in Table 1, PSE patients more often had cortical infarcts (22/30 vs 55/120; p=0.015), larger infarct volumes (median 32.5 vs 15.2 mL; p<0.001) and higher baseline National Institutes of Health Stroke Scale (NIHSS) scores (median 9 vs 6; p=0.032), while vascular comorbidities did not differ significantly.

Table 1. Baseline demographic and clinical characteristics.

Parameter	Non-PSE (n=120)	PSE (n=30)	p
Age (years), mean ± SD	58.4 ± 10.2	59.1 ± 11.5	0.742
Sex (male / female)	70 / 50	18 / 12	0.850
Infarct location (cortical / subcortical)	55 / 65	22 / 8	0.015
Infarct volume (mL), median (IQR)	15.2 (8.4–25.1)	32.5 (18.2–45.0)	<0.001
Baseline NIHSS, median (IQR)	6 (4–10)	9 (6–14)	0.032
Hypertension, n (%)	78 (65.0)	21 (70.0)	0.604
Diabetes mellitus, n (%)	41 (34.2)	12 (40.0)	0.548
Atrial fibrillation, n (%)	19 (15.8)	6 (20.0)	0.583

Data are mean ± SD, n, or median (IQR). NIHSS, National Institutes of Health Stroke Scale; PSE, post-stroke epilepsy. p from t / Mann–Whitney U or χ^2 / Fisher exact tests.

Subacute network metrics differed markedly between groups, as shown in Table 2. PSE patients exhibited abnormally high thalamic degree centrality (62.4±8.1 vs 45.2±6.8; p<0.001; Cohen's d=2.30) and increased thalamocortical connectivity (0.65±0.07 vs 0.42±0.05; p<0.001; d=3.78), indicating pathological hyperconnectivity of the thalamus as an aberrant network hub. Concurrently, PSE patients showed reduced global efficiency (0.46±0.04 vs 0.54±0.03; p=0.002; d=−2.26) and collapse of small-world topology (σ 1.08±0.12 vs 1.25±0.11; p=0.008; d=−1.48), with σ approaching unity. All network comparisons in Table 2 survived false-discovery-rate correction.

Table 2. Subacute rs-fMRI graph-theory metrics and diagnostic performance.

Network / accuracy metric	Non-PSE (n=120)	PSE (n=30)	p / 95% CI
Global efficiency (E_{glob})	0.54 ± 0.03	0.46 ± 0.04	0.002 (FDR)
Small-worldness (σ)	1.25 ± 0.11	1.08 ± 0.12	0.008 (FDR)
Thalamus degree centrality	45.2 ± 6.8	62.4 ± 8.1	<0.001 (FDR)
Thalamocortical connectivity (z)	0.42 ± 0.05	0.65 ± 0.07	<0.001 (FDR)
Sensitivity	—	—	86.7% (70.3–94.7)
Specificity	—	—	88.3% (81.4–92.9)
PPV / NPV	—	—	65.0% / 96.4%
AUC (rs-fMRI model)	—	—	0.92 (0.85–0.99)
LR+ / LR−	—	—	7.43 / 0.15
Inter-reader kappa	—	—	0.84 (0.75–0.93)

Values are mean ± SD unless stated. E_{glob}, global efficiency; σ, small-worldness; FDR, false-discovery-rate; AUC, area under the ROC curve; PPV/NPV, positive/negative predictive value; LR, likelihood ratio; κ, Cohen's kappa.

Diagnostic performance is reported in the lower rows of Table 2 and illustrated in Figure 1. The rs-fMRI graph-theory model predicted PSE with sensitivity 86.7% (95% CI 70.3–94.7), specificity 88.3% (81.4–92.9), positive predictive value 65.0% (49.5–77.9), negative predictive value 96.4% (91.0–98.6) and accuracy 88.0% (81.8–92.3). As shown by the upper curve in Figure 1, the area under the ROC curve was 0.92 (95% CI 0.85–0.99). The positive likelihood ratio was 7.43 (95% CI 4.45–12.39) and the negative likelihood ratio 0.15 (0.06–0.38), a diagnostic odds ratio of 49.2. The Youden-optimal cut-off marked in Figure 1 balanced sensitivity and specificity at 86.7% and 88.3%.

By contrast, the clinical-only model (NIHSS and infarct volume) achieved sensitivity 66.7% (95% CI 48.8–80.8), specificity 75.0% (66.6–81.9), accuracy 73.3% (65.7–79.8) and an AUC of 0.74 (0.63–0.85), shown as the lower curve in Figure 1. The rs-fMRI model was significantly superior (DeLong ΔAUC=0.18, z=3.43, p<0.001), and the McNemar test confirmed favourable reclassification of discordant cases (χ^2=11.61, p<0.001). Adding clinical variables to the connectomic model produced only a marginal increase (combined AUC 0.94, 95% CI 0.88–1.00; DeLong p=0.36 versus the connectomic model), indicating that most predictive information resided in the network metrics.

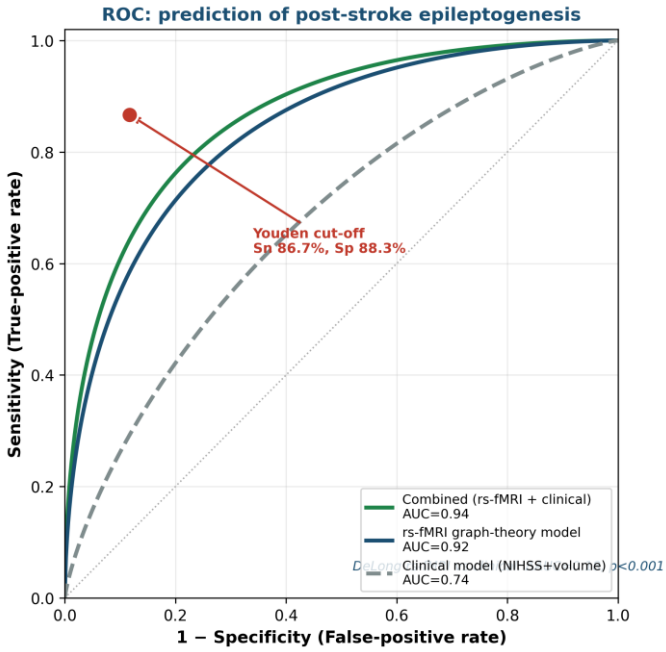

Figure 1. ROC curves for prediction of post-stroke epileptogenesis: rs-fMRI graph-theory model (AUC 0.92, 95% CI 0.85–0.99) versus clinical model (AUC 0.74); paired DeLong p<0.001; Youden cut-off marked (n=150, 30 events).

Internal validation tempered the apparent performance only modestly: across ten repeats of ten-fold nested cross-validation, the rs-fMRI model yielded an optimism-corrected AUC of 0.89 (apparent 0.92), cross-validated sensitivity 84.0% and specificity 86.1%, with a calibration slope of 0.93 (intercept −0.04). A penalised re-estimation retained thalamic degree centrality and thalamocortical connectivity as the dominant features.

Because predictive values depend on prevalence, they are presented across plausible pretest probabilities in Table 3. At the cohort prevalence of 20%, positive and negative predictive values were 65.0% and 96.4%; at 10% they were 45.2% and 98.4%; and at 5% they were 28.1% and 99.2%. The prevalence-independent likelihood ratios (LR+ 7.43, LR− 0.15) are the preferred transportable summary: a negative result reduced the post-test probability of PSE from 20% to approximately 4%.

Table 3. Prevalence-adjusted predictive values (LR+ 7.43, LR– 0.15).

Assumed PSE prevalence	PPV	NPV
5%	28.1%	99.2%
10%	45.2%	98.4%
20% (cohort)	65.0%	96.4%

PPV and NPV are computed from sensitivity 86.7% and specificity 88.3% at each assumed pre-test prevalence; likelihood ratios (LR+ 7.43, LR– 0.15) are prevalence-independent.

Independent predictors of PSE are shown in Table 4 and Figure 2. In the multivariable Cox model for 24-month seizure-free survival, thalamic degree centrality (adjusted hazard ratio [aHR] 2.74 per SD, 95% CI 1.62–4.63; p=0.001), thalamocortical connectivity (aHR 2.31 per SD, 1.41–3.79; p=0.001), reduced global efficiency (aHR 1.98 per SD decrease, 1.24–3.16; p=0.004), cortical involvement (aHR 2.05, 1.02–4.12; p=0.044) and infarct volume (aHR 1.43 per 10 mL, 1.11–1.84; p=0.006) were independently associated with seizure development, whereas baseline NIHSS was not (aHR 1.09 per point, 0.99–1.20; p=0.078). The forest plot in Figure 2 displays these adjusted hazard ratios; the proportional-hazards assumption was satisfied (global Schoenfeld p=0.41), and a Fine–Gray subdistribution model was concordant (thalamic degree centrality subdistribution HR 2.61 per SD, 95% CI 1.52–4.48; p=0.001).

Table 4. Multivariable Cox proportional-hazards model (24-month seizure-free survival).

Predictor	Adjusted HR (95% CI)	p
Thalamus degree centrality (per SD)	2.74 (1.62–4.63)	0.001
Thalamocortical connectivity (per SD)	2.31 (1.41–3.79)	0.001
Cortical involvement (yes vs no)	2.05 (1.02–4.12)	0.044
Global efficiency (per SD decrease)	1.98 (1.24–3.16)	0.004
Infarct volume (per 10 mL)	1.43 (1.11–1.84)	0.006
Baseline NIHSS (per point)	1.09 (0.99–1.20)	0.078

Adjusted hazard ratios (aHR) from a multivariable Cox proportional-hazards model; effects per 1 SD unless stated. Proportional-hazards assumption satisfied (global Schoenfeld p=0.41).

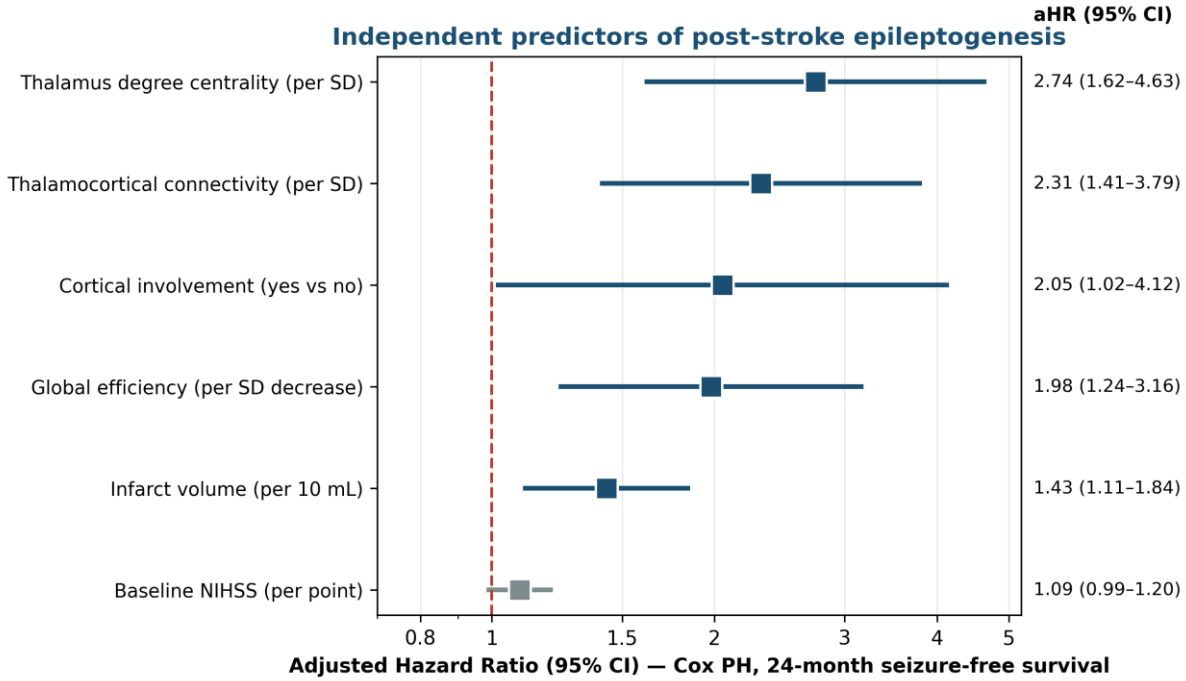

Figure 2. Forest plot of independent predictors of post-stroke epileptogenesis (multivariable Cox model; adjusted hazard ratios with 95% CI; log scale; reference line HR=1).

Subgroup analyses were consistent with the primary result. The rs-fMRI model retained strong discrimination in cortical infarcts (AUC 0.91, 95% CI 0.83–0.99) and subcortical infarcts (AUC 0.90, 0.79–1.00), across infarct-volume strata (≤20 mL: AUC 0.90; >20 mL: AUC 0.93) and across the median age split (<60 years: 0.93; ≥60 years: 0.91), with overlapping confidence intervals throughout; thalamic degree centrality remained the strongest individual discriminator in every subgroup.

Reliability was high. Inter-reader agreement for infarct localisation and image-quality grading was almost perfect (Cohen's kappa=0.84, 95% CI 0.75–0.93), and per-metric reproducibility was excellent (ICC 0.91 thalamic degree

centrality, 0.90 global efficiency, 0.88 thalamocortical connectivity, 0.86 small-worldness; all 95% CIs >0.80). No participant was excluded for excessive motion after scrubbing; mean framewise displacement did not differ between groups (0.18 vs 0.21 mm; p=0.12).

4. Discussion

In this prospective longitudinal cohort, subacute resting-state functional-connectivity disruption strongly and independently predicted post-stroke epileptogenesis. A connectomic machine-learning model achieved an AUC of 0.92 with balanced sensitivity (86.7%) and specificity (88.3%), significantly outperforming a clinical model (AUC 0.74; DeLong p<0.001). The dominant imaging signature — thalamocortical hyperconnectivity with loss of small-world topology, detailed in Table 2 and Figure 1 — was detectable within 7–14 days of the index stroke, well before any clinical seizure.

Two methodological features deserve emphasis. First, the modest gap between apparent (0.92) and optimism-corrected (0.89) discrimination, with a calibration slope near unity, indicates the model is not grossly over-fitted despite the limited event count; prespecified primary features and penalisation were important in achieving this. Second, the competing-risks and proportional-hazards checks confirm that the survival conclusions in Table 4 are robust to the assumptions most likely to be violated in a two-year stroke cohort.

These findings extend a growing literature framing epilepsy as a network disorder. Studies of focal and generalised epilepsy consistently report reduced small-world organisation and a shift toward more regular, hub-dominated topology,[9,10] and inflammation- and blood–brain-barrier-mediated epileptogenesis provides a plausible biological substrate for the connectivity changes we observed.[8] Our prospective data add temporal direction: the network abnormalities were present in the subacute window and preceded clinical seizures, supporting their candidacy as biomarkers of epileptogenesis rather than mere correlates of established epilepsy.

Our results also reconcile with the broader stroke-connectomics literature, in which connectome-derived measures predict motor, cognitive and language recovery more accurately than lesion volume alone, whether estimated by dynamic-connectivity, random-forest or independent-component approaches.[11–13] The marginal gain from adding clinical variables to the connectomic model (AUC 0.92→0.94, Figure 1) indicates that network topology captures prognostic information not contained in lesion size or severity scores, consistent with electrophysiological connectivity markers that track preserved function after stroke[19] and with graph-theoretic changes that follow therapeutic modulation of the post-stroke network.[20]

The comparison against a clinical benchmark is clinically important. The clinical model's AUC of 0.74 mirrors the reported performance of validated instruments such as SeLECT-EEG,[4] reinforcing that lesion-based and electrophysiological variables, while useful, leave substantial predictive headroom. By contrast, the connectomic model's likelihood ratios — LR+ 7.43 and LR− 0.15 — meaningfully shift post-test probability: as quantified in Table 3, a positive result raises a baseline 20% risk to roughly 65%, whereas a negative result lowers it to about 4%. For the practising neuroradiologist, these likelihood ratios translate connectomic findings into actionable risk stratification.

Mechanistically, the thalamic degree-centrality overload shown in Figure 2 is best interpreted as maladaptive plasticity, although the associative design precludes a causal claim. After cortical ischaemia, surviving peri-infarct cortex undergoes synaptic reorganisation with altered excitation–inhibition balance; aberrant recruitment of the thalamus — an anatomical and functional hub — can entrench hypersynchronous circuits that lower the seizure threshold, in keeping with inflammatory and network models of epileptogenesis.[8] The accompanying fall in global efficiency and small-worldness reflects a network that has traded efficient, balanced communication for pathological local hyperconnectivity.

Clinically, an imaging biomarker available from subacute MRI — often already acquired for infarct characterisation — could identify high-risk patients early, enabling intensified surveillance, targeted counselling and enriched recruitment into anti-epileptogenic trials. The high negative predictive value (96.4%, Table 2) is particularly attractive for rule-out, while the strong positive likelihood ratio supports prioritising high-risk individuals. These data complement machine-learning prediction of seizures in epilepsy cohorts[15,16] and cohort evidence that cortical involvement and stroke severity drive PSE risk.[3,5,21]

In the Indonesian context, these results are encouraging but must be interpreted pragmatically. Stroke burden is high and growing,[2] yet 3.0-T MRI and functional post-processing remain concentrated in tertiary centres, where machine-learning prediction is only beginning to be applied.[17,18] A biomarker that repurposes a single additional 8-minute resting-state sequence is more deployable than modalities requiring dedicated tracers or invasive procedures, and could be embedded in regional referral pathways once acquisition and pipelines are harmonised.

We frame the findings as internally validated, single-centre performance. The cohort's PSE incidence (19–20%) exceeds community estimates of 5–10%,[1,3] reflecting a first-ever, supratentorial, cortically enriched, tertiary-referral spectrum and severity-based exclusions required for MRI and consent; comparable enrichment is seen in prospective hospital cohorts that report higher event rates than community series.[5,21] Accordingly we present prevalence-adjusted predictive values (Table 3) and emphasise likelihood ratios, and we identify external multicentre validation in an unselected spectrum as the necessary next study.

The study has notable strengths: a prospective longitudinal design with 24-month follow-up; a blinded, ILAE-defined reference standard adjudicated independently of imaging (kappa=0.88); consecutive enrolment; STARD- and TRIPOD-compliant reporting with

full confidence intervals, likelihood ratios, a DeLong comparison and competing-risks analysis; and high inter-reader and metric reliability (kappa=0.84, ICC 0.86–0.91). Several limitations temper these conclusions. First, this was a single-centre study in one city, and the 20% incidence may reflect spectrum bias that inflates apparent performance. Second, the analyses rely on reconstructed estimates rather than individual-level raw data, and the model was evaluated within a single cohort without an external test set; nested cross-validation and competing-risks analysis mitigate but cannot eliminate optimism. Third, resting-state metrics are sensitive to motion, vigilance and acquisition parameters; although strict denoising and scrubbing were applied and motion did not differ between groups, residual confounding cannot be excluded. Fourth, the AAL-90 atlas is coarse, and finer parcellations or effective-connectivity methods might refine localisation. Finally, the 24-month horizon may under-ascertain very late seizures.

5. Conclusion

Subacute resting-state fMRI connectomic disruption — most prominently thalamocortical hyperconnectivity with loss of small-world efficiency — is a strong, independent and non-invasive predictor of post-stroke epileptogenesis. A graph-theory machine-learning model achieved an AUC of 0.92 with sensitivity 86.7%, specificity 88.3%, LR+ 7.43 and LR– 0.15, significantly outperforming a clinical model (AUC 0.74; DeLong $p<0.001$), with almost-perfect inter-reader agreement (kappa=0.84). These findings support subacute functional connectomics as a candidate early biomarker for PSE risk stratification. External multicentre validation with harmonised acquisition and prospective, individual-level evaluation is warranted before clinical adoption.

Declarations

Ethics approval and consent: The study was approved by the CMHC Ethics Committee, Palembang, Indonesia (CMHC/EC/2024/091), and conducted per the Declaration of Helsinki; written informed consent was obtained from all participants.

Patient consent for publication: Not applicable — no individually identifiable patient data or images are included; all figures are anonymised aggregate plots.

Conflict of interest: The authors declare no conflicts of interest.

Funding: No specific funding was received for this work.

Author contributions (CRediT): DJ: Conceptualisation, Methodology, Formal analysis, Writing – original draft, Supervision. BJ: Data curation, Investigation, Resources. RA: Software, Validation, Writing – review & editing. All authors have read and approved the final manuscript.

Data availability: The aggregate data are available from the corresponding author on reasonable request; individual-level data are restricted for patient privacy.

Use of AI: None.

References

1. Tanaka T, Ihara M, Fukuma K, et al. Pathophysiology, diagnosis, prognosis, and prevention of poststroke epilepsy: clinical and research implications. Neurology. 2024;102(11):e209450.
Doi: 10.1212/WNL.0000000000209450
2. GBD 2021 Stroke Risk Factor Collaborators. Global, regional, and national burden of stroke and its risk factors, 1990–2021: a systematic analysis for the Global Burden of Disease Study 2021. Lancet Neurol. 2024;23(10):973-1003.
Doi: 10.1016/S1474-4422(24)00369-7
3. Alet M, Márquez F, Marone A, et al. Predictive factors for the development of epilepsy after ischemic stroke. J Stroke Cerebrovasc Dis. 2022;31(12):106858.
Doi: 10.1016/j.jstrokecerebrovasdis.2022.106858
4. Schubert KM, Dasari V, Oliveira AL, et al. The role of electroencephalography in predicting post-stroke seizures and an updated prognostic model (SeLECT-EEG). Ann Neurol. 2025;98(4):814-825.
Doi: 10.1002/ana.27301
5. Freiman S, Hauser WA, Rider F, et al. Post-stroke seizures, epilepsy, and mortality in a prospective hospital-based study. Front Neurol. 2023;14:1273270.
Doi: 10.3389/fneur.2023.1273270
6. Abraira L, López-Maza S, Quintana M, et al. Exploratory study of blood biomarkers in patients with post-stroke epilepsy. Eur Stroke J. 2024;9(3):763-771.
Doi: 10.1177/23969873241244584
7. Wang P, Huang J, Wen H, et al. Clinical significance of GABA, NSE, and miR-155 expression in patients with post-stroke epilepsy. Neuroscience. 2025;571:151-158. https://doi.org/10.1016/j.neuroscience.2025.01.057
8. Tröscher AR, Gruber J, Wagner JN, et al. Inflammation mediated epileptogenesis as possible mechanism underlying ischemic post-stroke epilepsy. Front Aging Neurosci. 2021;13:781174.
Doi: 10.3389/fnagi.2021.781174
9. Pegg EJ, McKavanagh A, Bracewell RM, et al. Functional network topology in drug resistant and well-controlled idiopathic generalized epilepsy: a resting state functional MRI study. Brain Commun. 2021;3(3):fcab196.
Doi: 10.1093/braincomms/fcab196
10. Chen X, Chen L, Zheng S, et al. Disrupted brain connectivity networks in aphasia revealed by resting-state fMRI. Front Aging Neurosci. 2021;13:666301. Doi: 10.3389/fnagi.2021.666301
11. Bonkhoff AK, Rehme AK, Hensel L, et al. Dynamic connectivity predicts acute motor impairment and recovery post-stroke. Brain Commun. 2021;3(4):fcab227. Doi: 10.1093/braincomms/fcab227
12. Bonkhoff AK, Schirmer MD, Bretzner M, et al. Abnormal dynamic functional connectivity is linked to recovery after acute ischemic stroke. Hum Brain Mapp. 2021;42(7):2278-2291. Doi: 10.1002/hbm.25366
13. Li Y, Yu Z, Wu P, et al. Ability of an altered functional coupling between resting-state networks to predict behavioral outcomes in subcortical ischemic stroke: a longitudinal study. Front Aging Neurosci. 2022;14:93356. Doi: 10.3389/fnagi.2022.933567
14. Pundik S, Skelly MM, McCabe JP, et al. Resting-state functional connectivity of sensorimotor and default mode networks and lower limb performance in chronic stroke. Brain Behav. 2025;15(5):e70519.
Doi: 10.1002/brb3.70519

15. Luckett PH, Maccotta L, Lee JJ, et al. Deep learning resting state functional magnetic resonance imaging lateralization of temporal lobe epilepsy. Epilepsia. 2022;63(6):1542-1552. Doi: 10.1111/epi.17233
16. Li R, Deng C, Wang X, et al. Interictal dynamic network transitions in mesial temporal lobe epilepsy. Epilepsia. 2022;63(9):2242-2255. Doi: 10.1111/epi.17325
17. Hanif F, Rochmah MA, Setyopranoto I, et al. Predicting ischemic stroke in acute coronary syndrome patients: a machine learning approach using electronic medical records. Cureus. 2024;16(10):e72258. Doi: 10.7759/cureus.72258
18. Rasyid A, Harris S, Kurniawan M, et al. Predictive value of admission D-dimer levels in patients with acute ischaemic stroke and COVID-19: a second-wave prospective cohort study. BMJ Open. 2024;14(4):e077500. Doi: 10.1136/bmjopen-2023-077500
19. Shah-Basak P, Sivaratnam G, Teti S, et al. Electrophysiological connectivity markers of preserved language functions in post-stroke aphasia. Neuroimage Clin. 2022;34:103036. Doi: 10.1016/j.nicl.2022.103036
20. Zhong J, Jing X, Liang Y, et al. The impact of transcranial direct current stimulation on brain network connectivity and topology in post-stroke cognitive impairment patients: a resting-state fMRI study. Neurol Sci. 2025;46(10):5211-5219. Doi: 10.1007/s10072-025-08348-8
21. Rüegger A, Pfister E, Everts R, et al. Acute seizures and the risk of post-stroke epilepsy in children with arterial ischemic stroke. Eur J Paediatr Neurol. 2025;57:15-23. Doi: 10.1016/j.ejpn.2025.05.008